Journal of Microwave Power and Electromagnetic Energy

ISSN: 0832-7823 (Print) Journal homepage: www.tandfonline.com/journals/tpee20

Characterization of microwave plasma for electromagnetic modeling in processing applications

Camille E. Williams & Vadim V. Yakovlev

To cite this article: Camille E. Williams & Vadim V. Yakovlev (2025) Characterization of microwave plasma for electromagnetic modeling in processing applications, Journal of Microwave Power and Electromagnetic Energy, 59:2, 170-194, DOI: 10.1080/08327823.2025.2490434

To link to this article: https://doi.org/10.1080/08327823.2025.2490434

JOURNAL OF MICROWAVE POWER AND ELECTROMAGNETIC ENERGY
2025, VOL. 59, NO. 2, 170–194
https://doi.org/10.1080/08327823.2025.2490434

RESEARCH ARTICLE

Characterization of microwave plasma for electromagnetic modeling in processing applications

Camille E. Williams[a,b] and Vadim V. Yakovlev[a]

[a]Center for Industrial Mathematics and Statistics, Department of Mathematical Sciences, Worcester Polytechnic Institute, Worcester, Massachusetts, USA; [b]Department of Physics, Worcester Polytechnic Institute, Worcester, Massachusetts, USA

ABSTRACT
Computer modeling is a powerful tool for the design of systems and processes of microwave power engineering; however, its application to devices containing plasma is still limited. Electromagnetic properties of plasma are difficult to measure, and their dependence on operational parameters of the device are system dependent. In this paper, we describe a simple model in which microwave plasma is represented by electric conductivity, frequency of electron-neutral collisions, and plasma frequency. These characteristics are compatible with input media parameters of the finite-difference time-domain (FDTD) technique. To overcome the uncertainty for input generation, we use a series of assumptions to link the input parameters to electron density, average electron velocity, electron collision cross-section, gas temperature, electron temperature, and further, to microwave power and pressure. We discuss the steps to approximate the input parameters based on available data or informed calculations. We demonstrate this approach for an FDTD model of a cylindrical cavity containing plasma in a coaxial quartz vessel and validate the model against analytical results. Simulated patterns of the electric field and frequency responses of the reflection coefficient show that the proposed approach may be practical for determining the operational bounds of applicators with plasma and assisting in their CAD.

ARTICLE HISTORY
Received 14 November 2024
Accepted 28 March 2025

KEYWORDS
Conductivity; electron collision frequency; electron density; FDTD modeling; microwave plasma; microwave power; plasma frequency; pressure

1. Introduction

Applications of microwave (MW) plasma in processing technologies (Mehdizadeh 2015; Toyoda 2020; Bardos and Barankova 2022) include artificial diamond production (Silva et al. 2009; Thomas et al. 2018; Bardos and Barankova 2022), surface processing for semiconductor components (e.g. deposition, etching, cleaning) (Ventzek et al. 2002; Shearn et al. 2010; Pauly et al. 2022), and plasma-based decomposition of CO_2 (Ashford and Tu 2017; Ong et al. 2022), among others. However, experimental development of efficient and controllable applicators is challenging (Bardos

CONTACT Vadim V. Yakovlev vadim@wpi.edu Center for Industrial Mathematics and Statistics, Department of Mathematical Sciences, Worcester Polytechnic Institute, Worcester, MA, USA.
Supplemental data for this article can be accessed online at https://doi.org/10.1080/08327823.2025.2490434.

and Barankova 2022). While examples of computer simulations which assist in the design of such systems are widely reported (Silva et al. 2009; Diaz 2011; Nowakowska et al. 2011a; 2011b; Shivkumar et al. 2016; Xiao et al. 2016; Latrasse et al. 2017; Zhang et al. 2017; Shen et al. 2020; Wu et al. 2021; Yadav et al. 2021; Pauly et al. 2022; Xiao et al. 2022a; 2022b; Chen et al. 2023; Zhong et al. 2023), the use of advanced modeling and CAD remains limited by a principal data uncertainty in characterizing MW plasma for electromagnetic (EM) models. One option is to characterize plasma using the complex permittivity, but it is difficult to directly measure (Li et al. 2018; Wang et al. 2021), and its relationship to controllable device parameters is system dependent. The complex permittivity of plasma can be estimated by theoretical calculation (Wang et al. 2021; Xiao et al. 2022a), but a systematic approach to go about this is insufficiently developed. The substantial complexity of the underlying physics is in part responsible for this drawback.

In this paper – expanding on the initial ideas outlined in Williams and Yakovlev (2023) – we describe a simple model in which MW plasma is characterized succinctly by the electric conductivity and is conditioned by the frequency of electron-neutral collisions and the plasma frequency. We provide the rationale for all necessary approximations and discuss the hierarchy of plasma parameters and their connection to parameters of the applicator (i.e. MW power, pressure, and the gas flow rate). To bridge the principal data uncertainty, our suggestion is that, for a choice of neutral gas, the set of input data may be calculated using electron density, neutral gas density, and average electron velocity. If these values are not easily acquired, they can be plausibly assumed by consulting literature for similar MW applicators.

The proposed plasma model is made fully compatible with the finite-difference time-domain (FDTD) technique as implemented in the full-wave EM simulation software *QuickWave*™ (QuickWave 1998–2024), whereas the previous studies modeling systems with MW plasma (Nowakowska et al. 2011a; 2011b; Xiao et al. 2016; Latrasse et al. 2017; Zhang et al. 2017; Pauly et al. 2022; Xiao et al. 2022a; Chen et al. 2023; Yadav et al. 2023; Zhong et al. 2023) have employed *COMSOL Multiphysics*® (COMSOL Multiphysics 1998–2023) based on the finite element method (FEM). With respect to complex MW structures (in particular, high-power applicators), FDTD EM modeling has proven to be computationally beneficial (Yakovlev 2006; Celuch and Gwarek 2007; Yakovlev et al. 2011; Celuch et al. 2020; Kumi et al. 2020; Porter et al. 2023) and is better suited for CAD and optimization of applied systems in research and industrial applications.

Following the proposed approach, we compile appropriate input values and demonstrate the simulation of a simple system resembling some common applicators containing plasma. Computational results of this survey clearly show well-known behavior of the electric field in the presence of plasma with frequencies above and below the frequency of the microwave field (critical electron density). This confirmation supports the legitimacy of the proposed plasma model. Simulated frequency characteristics of the reflection coefficient also suggest that the energy efficiency of MW applicators with plasma depends on multiple device and plasma parameters. Relevant EM modeling may help better understand the role of these parameters in applicator operation.

The overall objectives of the present study are therefore to (*i*) propose a simple approach for the generation of input data on plasma medium for FDTD EM modeling of microwave applicators (with potential for further development), (*ii*) discuss the validity of the proposed characterization, and (*iii*) demonstrate, through illustrative simulations, the possible benefits of FDTD modeling output for research and development of microwave plasma devices.

2. Background: conductivity-based model of microwave plasma

2.1. Lorentz model

The Lorentz model describes the behavior of electrons in a material under the influence of an electric field (Almog et al. 2011). It assumes that the electrons are both significantly less massive than the nuclei of the material, and that they are coupled to the nuclei by a spring-like force. When an electric field $\boldsymbol{E}$ is induced, the displacement of electrons by $\boldsymbol{r}$ creates a polarization in the material. Using a collection of established concepts (Griffiths 2020), it is possible to extrapolate the complex permittivity, and thus the electric conductivity of the material.

In the Lorentz model, oscillation of the electrons is described using a second-order differential equation with respect to time:

$$m\frac{\partial^2 \boldsymbol{r}(t)}{\partial t^2} = -m\omega_o^2 \boldsymbol{r}(t) - m\gamma\frac{\partial \boldsymbol{r}(t)}{\partial t} - q\boldsymbol{E}(t) \tag{1}$$

where m is the mass of an electron, ω_0 is the angular frequency of the spring-like force, γ is the electron heavy-particle collision frequency for momentum transfer, q is the charge of an electron, and $\boldsymbol{E}$ is the applied electric field. For the purposes of this model, ω_0 represents the restoration of electrons to their neutral position proportional to the strength of the Coulomb force between electron and nuclei. The first term on the right-hand side of Eq. (1) represents the restorative spring force. The second term is the damping force and is conditioned by the collision of electrons and heavy particles (Heald 1965). The third term is the driving force of the system. Cumulatively, these forces equal the left side of Eq. (1) *via* Newton's second law. Equation (1) can be rewritten in standard form as:

$$\frac{\partial^2 \boldsymbol{r}(t)}{\partial t^2} + \gamma\frac{\partial \boldsymbol{r}(t)}{\partial t} + \omega_o^2 \boldsymbol{r}(t) - = -\frac{q}{m}\boldsymbol{E}(t). \tag{2}$$

Applying a Fourier transform uniformly to (2), the result is rearranged to give the displacement of electrons $\widehat{R}$ as a function of angular frequency ω:

$$\widehat{\boldsymbol{R}}(\omega) = \left(-\frac{q}{m}\right)\left[\frac{1}{\omega_o^2 - \omega^2 + i\gamma\omega}\right]\widehat{\boldsymbol{E}}(\omega). \tag{3}$$

where $\widehat{E}$ is the Fourier transformed electric field. $\widehat{R}$ is related to the dipole moment μ by

$$\mu(\omega) = -q\cdot\widehat{\boldsymbol{R}}(\omega). \tag{4}$$

and

$$\boldsymbol{p}(\omega) = N \cdot \boldsymbol{\mu}(\omega) \tag{5}$$

where $\boldsymbol{p}$ is the macroscopic polarization (dipole moment per unit volume), and N is the electron density. Using Eqs. (4) and (5) to solve for $\boldsymbol{p}$,

$$\boldsymbol{p}(\omega) = \left(\frac{Nq^2}{m}\right)\left[\frac{1}{\omega_o^2 - \omega^2 + i\gamma\omega}\right]\boldsymbol{E}(\omega). \tag{6}$$

Polarization is related to electric susceptibility χ_e by

$$\boldsymbol{p}(\omega) = \varepsilon_o \chi_e \boldsymbol{E}(\omega), \tag{7}$$

where ε_o is the permittivity of free space. Substituting the expression (6) into (7), χ_e can be written as

$$\chi_e = \left(\frac{Nq^2}{m\varepsilon_o}\right)\left[\frac{1}{\omega_o^2 - \omega^2 + i\gamma\omega}\right]. \tag{8}$$

Finally, the relative complex permittivity is calculated by $\varepsilon_r = 1 + \chi_e$:

$$\varepsilon_r = 1 + \left(\frac{Nq^2}{m\varepsilon_o}\right)\left[\frac{1}{\omega_o^2 - \omega^2 + i\gamma\omega}\right]. \tag{9}$$

This expression is sufficient, but it can be effectively simplified by substituting an expression for plasma frequency ω_p given by the Appleton-Hartree equation which describes wave propagation in cold plasmas (like microwave plasma) (Almog et al. 2011; Toyoda 2020; Bardos and Barankova 2022):

$$\omega_p = \sqrt{\frac{Nq^2}{m\varepsilon_o}}. \tag{10}$$

A general expression for the relative complex permittivity of a material under the Lorentz model is therefore

$$\varepsilon_r = 1 + \frac{\omega_p^2}{\omega_o^2 - \omega^2 + i\gamma\omega}. \tag{11}$$

In cases with free electrons like metals or plasma, the Lorentz-Drude model is best applied. It describes a case of the Lorentz model such that the restorative force is zero, $\omega_o = 0$. The simplified expression for the relative complex permittivity becomes:

$$\varepsilon_r = 1 - \frac{\omega_p^2}{\omega^2 + i\gamma\omega}. \tag{12}$$

Furthermore,

$$\varepsilon_r = \varepsilon' - \varepsilon'', \tag{13}$$

such that the dielectric constant ε' and the loss factor ε'' are:

$$\varepsilon' = 1 - \frac{\omega_p^2}{\omega^2 + \gamma^2}, \tag{14}$$

and

$$\varepsilon'' = \frac{\omega_p^2 \gamma}{\omega(\omega^2 + \gamma^2)}, \tag{15}$$

respectively.

In applications, the operating frequency of MW systems $f = \omega/2\pi$ is generally constant and chosen to be one of the ISM frequencies. As a result, MW plasma can be characterized by two fundamental parameters: the electron collision frequency γ and the plasma frequency $f_p = \omega_p/2\pi$. These parameters are effectively included in the expression for electric conductivity σ (Grant 1958):

$$\sigma = \omega \varepsilon_o \varepsilon''. \tag{15}$$

The set of plasma parameters, σ, γ, and f_p, is consistent with input media parameters for dielectric dispersive materials in the *QuickWave* FDTD Lorentz-Drude dispersion model.

In the following sections, details of the electron collision frequency and plasma frequency are outlined, informing their connection to measurable parameters of the MW system.

2.2. Electron collision frequency

MW plasma is typically highly collisional and dominated by collisions between electrons and heavy particles (Green et al. 2001; Xiao et al. 2016; 2022a). Under these assumptions, the electron collision frequency γ can be approximated by the product of the neutral gas density n_g, the average thermal speed of the electrons v_e, and the cross-section of electron-neutral collisions σ_{en} (Heald and Wharton 1965; Green et al. 2001; Möller 2006):

$$\gamma = n_g v_e \sigma_{en}. \tag{16}$$

In Eq. (16), n_g can be approximated using the ideal gas equation (Pauly et al. 2022)

$$n_g = \frac{P}{k_B T_g}, \tag{17}$$

where P is the pressure of the plasma environment, k_B is the Kelvin-Boltzmann constant, and T_g is the gas temperature. Through its dependence on T_g, neutral gas density is determined by the shape of the plasma vessel, the MW power, and the gas flow rate (if applicable) (Green 2000; Jasinski and Zakrzewski 2002; Deng et al. 2017; Huang et al. 2022). It is also informatively correlated to electron density *via* the fractional degree of ionization I (Shang 2018):

$$n_g = \frac{N}{I} \tag{18}$$

This correlation is worth mentioning if I happens to be a more accessibly measurable device parameter than P, T_g, or n_g.

Furthermore, v_e in Eq. (16) can be approximated by the mean of the relevant Maxwell-Boltzmann distribution (Ling et al. 2016; Xiao et al. 2016; Toyoda 2020; Boulos et al. 2023)

$$v_e = \sqrt{\frac{8k_B T_e}{\pi m}}, \tag{19}$$

where that T_e is electron temperature. Through its dependence on T_e, v_e is determined by microwave power, pressure, and gas flow rate; these dependencies are studied in Masamba et al. (1992) and Derkaoui et al. (2014).

Finally, the electron collision cross-section σ_{en} can be loosely approximated by reducing collisions to be purely elastic between a point-charge electron and a heavy neutral gas ion. In this case, a simple expression can be used (Heald and Wharton, 1965):

$$\sigma_{en} = \pi r^2, \tag{20}$$

where r is the atomic radius of the neutral gas used to ignite the plasma. In reality, this parameter is complicated by a variety of particle interactions within the plasma. For example, polarization collisions are inelastic and are essential for the longevity of the plasma. Additionally, with the collision of charged particles, the impact parameter, and thus σ_{en}, depends on v_e (Heald and Wharton, 1965). In light of this complexity, Equation (20) serves as an appropriate simplification for the purposes of this analytical model. The values of r which are used are summarized in Clementi et al. (1967). To simplify the analysis, atoms are considered in isolation and their radii taken from theoretical models.

2.3. Plasma frequency

In accordance with (10), plasma frequency depends on electron density (such that $f_p \approx 8.968\sqrt{N}$). In reality, N is a spatially dependent parameter, with recognized phenomena such as the electron sheath contributing to its spatial variation. However, for simplicity of the baseline proposed model, it is treated as an average value across the plasma volume.

Electron density depends on pressure (Shirai et al 1999; Wu and Kou 1999; Hagelaar et al. 2004; Derkaoui et al. 2014; Latrasse et al. 2016), MW power (Shirai et al 1999; Hagelaar et al. 2004; Choi et al. 2007; Zhang et al. 2009; Baeva et al. 2012; Derkaoui et al. 2014; Latrasse et al. 2016; Xiao et al. 2016; Zhang et al. 2017; Klute et al. 2021; Xiao et al. 2022a; 2022b), and gas flow rate (if applicable) (Wu et al. 2021; Xiao et al. 2022a). Experimental results presented in the listed studies indicate that these dependencies are system dependent.

2.4. Electric conductivity

Summarizing the observations outlined in the previous subsections 2.2 and 2.3, the dependencies of the electron collision frequency and the plasma frequency on additional parameters are collectively presented in Figure 1. Plasma parameters, parameters of the MW device, and fundamental constants are highlighted in blue, orange, and green, respectively. Explicit connections such as f_p to electron density and γ to neutral gas density, average electron velocity, and the electron-neutral collision cross-section are represented using solid lines. Implicit connections that are system specific are represented by dotted lines. It is apparent that the electric conductivity of plasma depends on measurable system parameters, however, to generate inputs to the model from such parameters, some form of system-specific approximation or experimentation must take place.

The challenge with experimentally determining the roles of MW power, pressure, and flow rate is that the related measurements can require complex and expensive equipment. Such equipment would likely be unavailable if characterization of plasma were needed to assist in early stages of development or design. Therefore, depending

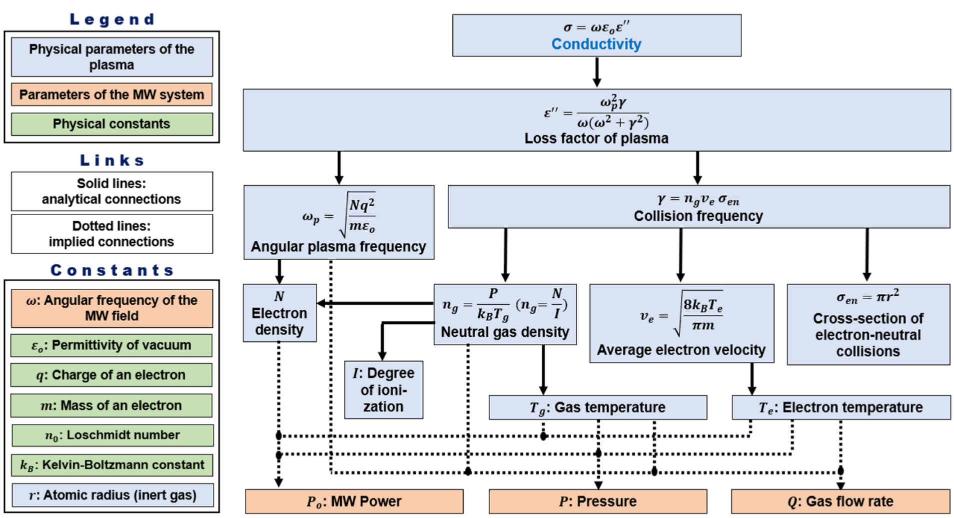

Figure 1. Characterization of electric conductivity of MW plasma through its physical parameters, fundamental constants, and parameters of the MW system.

on which parameters are most accessible by measurement (or lack thereof), the path to input parameters σ, γ, and f_p may differ. The flow chart seeks to inform the modeler/designer of multiple possible routes. In this paper, we assert that the required set of input data characterizing MW plasma may be compiled based on plausible values of N, n_g, and v_e. These parameters are chosen in accordance with reported data for similar MW applicators. σ_{en} is approximated using the selected neutral gas.

In Figure 2, the proposed approach for input generation is laid out in two phases. *Phase I* describes the link between device parameters and plasma parameters N, n_g, v_e, σ_{en}, bridged by either published or measured experimental data. *Phase II* two describes the explicit link between these plasma parameters and the input parameters σ, γ, and f_p. Phase II is calculated using a MATLAB script. The next section presents an illustrative example of this approach, provides detail on possible courses of action for choosing the input data, and highlights the usefulness and plausibility of the obtained modeling results.

3. FDTD EM modeling demonstration–microwave plasma system

3.1. FDTD inputs

In EM time-domain simulation, lossy media are characterized by electric conductivity. Based on the presented approach, to specify σ in the *QuickWave* FDTD model of a MW system containing plasma, one needs the electron collision frequency γ and the plasma frequency f_p to be specified (QuickWave 1998–2024).

3.1.1. Electron-neutral collision frequency

To obtain values for γ, we calculate them using Eq. (16) from parameters σ_{en}, n_g, and v_e.

The neutral gas density is determined by gas temperature and pressure (17). To obtain broadly instructive output from our simulation, it is therefore practical to evaluate data for gas temperature in both low and high (near-atmospheric) pressure scenarios. Muegge GmbH reports that in a variety of MW plasma applications, the value of the gas temperature is measured near 3,500 K (Muegge 2023). This is consistent with measured data in systems operating at near-atmospheric pressures (Green

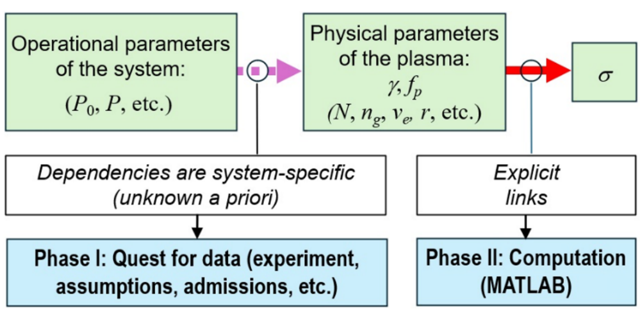

Figure 2. Conceptual profile of the proposed plasma model – a two-phase approach to determination of input data for EM FDTD modeling of MW systems with plasma.

at al. 2001; Zhang et al. 2009; Xiao et al. 2016; Deng et al. 2017). Adopting T_g = 3,500 K for near atmospheric applications, we can use (17) to calculate $n_g = 2.25{\cdot}10^{24}$ m^{-3}. For lower pressure processing applications, like in Pauly et al. (2022) (T_g = 373.15 K, $P = 160$ Pa), the value of neutral gas density can be appropriated as $n_g = 1.94{\cdot}10^{22}$ m^{-3}. With the latter approximation being two orders of magnitude lower, it demonstrates the importance of this distinction for different applications.

The average electron velocity is governed by the electron temperature (19). In Pauly et al. (2022), v_e was calculated based on T_e measured with Langmuir probes (1.9 eV), for a low-pressure MW plasma. Following (Schultze et al. 1998), in atmospheric plasmas, the electron temperature may be within 1 to 5 eV. Seeing that 1.9 eV is reflected in this range, we assume $v_e = 1.06{\cdot}10^6$ m/s is plausible for a variety of applications. This value was used to calculate γ for both low- and high-pressure scenarios in the demonstration that follows.

Values of the electron-neutral collision cross-sections can be calculated from (20) using the atomic radii of different neutral gases for which values are conveniently tabulated (Clementi et al. 1967). In our demonstration, γ is determined for a collection of gases known for their use for MW plasma ignition – Helium, Neon, Fluorine, Oxygen, Nitrogen, Argon, Krypton, and Xenon. These values of γ are detailed in Table 1.

3.1.2. Plasma frequency

Plasma frequency depends directly on electron density N, which differs significantly between low-pressure plasmas ($10^{16} < N < 10^{19}$ m^{-3}) and atmospheric pressure plasmas ($10^{20} < N < 10^{23}$ m^{-3}).

For any MW system containing plasma, there exists a critical plasma frequency f_{pc} which is equal to the operating frequency of the system f_0. This limiting behavior is occasionally referred to by the corresponding value of electron density N_c. The latter is normally one of the ISM frequencies, such as 0.915, 2.45, or 5.8 GHz. It has been widely demonstrated and well documented, including in Muegge (2023), that for plasma frequencies below f_{pc}, the electric field is able to penetrate the plasma domain, whereas above f_{pc} it quickly tapers off. We seek to demonstrate the behavior of the electric field near $f_{pc.}$ Setting f_0 = 2.45 GHz (so that $N_c = 7.6{\cdot}10^{16}$ m^{-3}), we vary f_p in the interval from 0.8 to 8.0 GHz (Figure 3).

3.1.3. Conductivity

Electric conductivity can be determined from the loss factor (15), which can be calculated from the prior two input parameters γ and f_p. Four surfaces in Figure 4 illustrate *Phase II* introduced in Figure 2 and demonstrate the behavior of plasma

Table 1. Calculated values of the collision frequency for typical inert gases at low pressure and near-atmospheric pressure.

Inert gas		He	Ne	F	N	O	Ar	Kr	Xe
r [pm] (Clementi et al. 1967)		31	38	42	48	56	71	88	108
γ [GHz]	$n_g = 1.94{\cdot}10^{22}$ m^{-3}	0.062	0.093	0.114	0.149	0.203	0.326	0.500	0.754
	$n_g = 2.25{\cdot}10^{24}$ m^{-3}	7.192	10.78	13.22	17.28	23.55	37.82	58.00	87.46

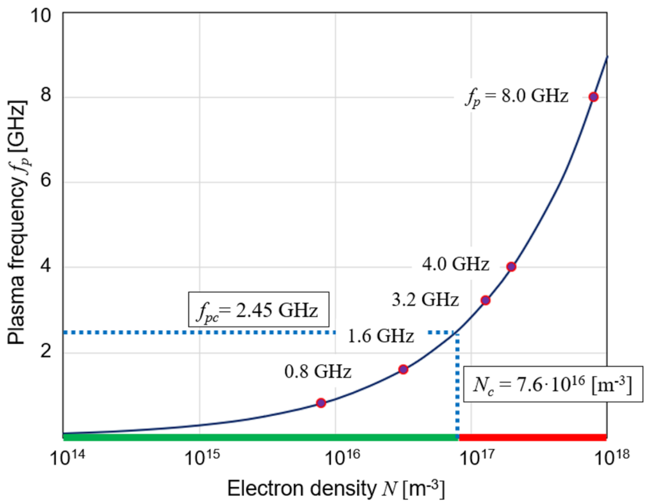

Figure 3. Plasma frequency as function of electron density in accordance with (10).

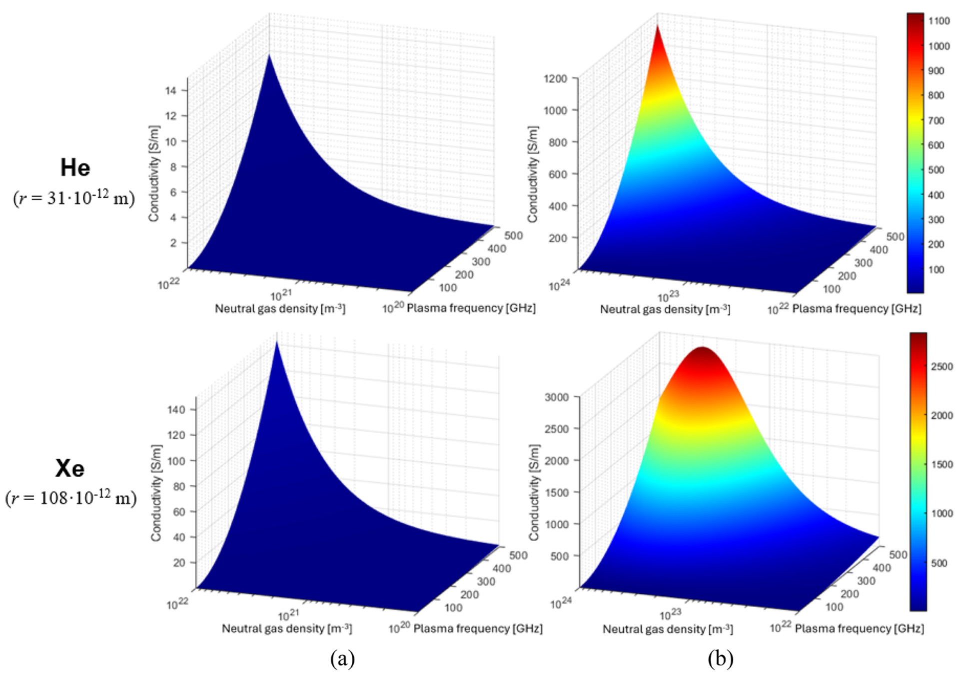

Figure 4. Electric conductivity of near-atmospheric (a) and atmospheric (b) plasma as function of plasma frequency and neutral gas density for He and Xe.

conductivity as function of the neutral gas density and plasma frequency. Both n_g (conditioned primarily by power) and f_p (conditioned primarily by pressure) are varied for Helium and Xenon characterized by the lowest and highest atomic radii in the chosen set. These graphs serve as a demonstration of how values of conductivity may be estimated in diverse plasma scenarios to assess EM performance of the MW system prior to its modeling.

3.2. FDTD model and its verification

To test the proposed characterization of MW plasma, we developed a model of a simple 2.45 GHz system resembling typical MW applicators containing plasma (Lebedev 2010; Latrasse et al. 2017; Bardos and Barankova 2022; Pauly et al. 2022). The system consists of a metal cylinder and coaxially placed quartz vessel containing a neutral gas where the plasma is ignited. It is fed by either a cross-sectionally, or longitudinally oriented rectangular waveguide (Figure 5). The geometric parameters are $D = 94$ mm, $d = 47$ mm, $L = 240$ mm, $l = 220$ mm, and $t = 1.5$ mm.

The waveguide used in excitation is WR284 (86×43 mm). Built for the full-wave FDTD simulator *QuickWave*, the model exploits a non-uniform mesh with 2.0 mm cells in air and 1.5 mm cells in quartz and plasma.

The applicator without the quartz vessel can be interpreted as a short section of an empty circular waveguide. In the model, this is emulated by setting the complex permittivity of the vessel walls to that of air. The model with these material parameters, $D = 130$ mm, and $L = 240$ mm was validated against analytical results in accordance with the approach described in Yakovlev (2018).

Each of the two waveguide orientations excites its own sets of modes. Three resonant frequencies computed by the *QuickWave* model agree well with the eigen frequencies of certain higher-order TE_{mn} and TM_{mn} modes in a circular waveguide with the same values of D and L. The details of this comparison are given in Table 2. The indices m and n were determined by computing the field at the resonant frequencies corresponding to the eigen frequencies and visually analyzing the field profiles. The similarities seen in Table 2 between analytically determined and modeled values suggest that the FDTD model of the system in Figure 5 produces reliable results.

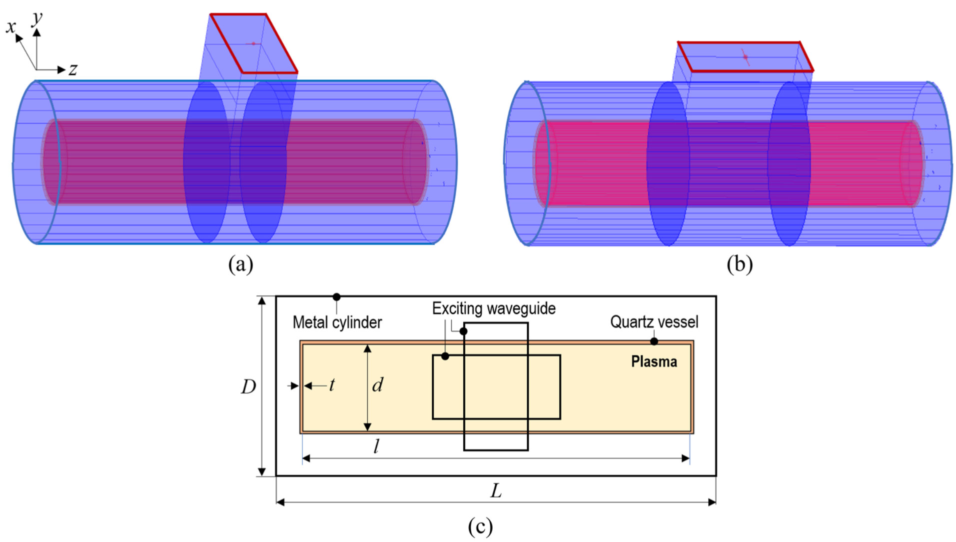

Figure 5. 3D views of the modeled cylindrical cavities with cross-sectional (a) and longitudinal (b) excitations by a rectangular waveguide and a coaxial quartz vessel (containing plasma) and the dimensions of all the elements (c).

3.3. Electric field patterns

Figures 6 and 7 show the simulated distributions of the electric field in the applicator (Figure 5) for both cross-sectional and longitudinal excitations, three different gases, and both high- and low-pressure values of neutral gas density n_g. In each case, a set of fields was obtained for five plasma frequencies over the interval of 1.6 to 3.2 GHz. This interval contains the critical plasma frequency which is equal to the operating frequency $f_0 = 2.45$ GHz. Each distribution in the xz-coordinate plane is shown with the maximum magnitude of the electric field $|E|_{max}$ and is normalized to the value of $|E|_{max}$ for $f_p = 1.6$ GHz (the largest magnitude amongst each set).

Table 2. Resonant frequencies of the modes excited in the empty system in Figure 5 and cutoff frequencies of the corresponding waveguide.

		Indices		Frequency (GHz)	
Excitation	Mode	*m*	*n*	Eigenvalue	Excited
Cross-sectional	TM	1	1	2.81	2.84
Cross-sectional	TM	2	1	3.77	3.78
Longitudinal	TE	4	1	3.85	3.91

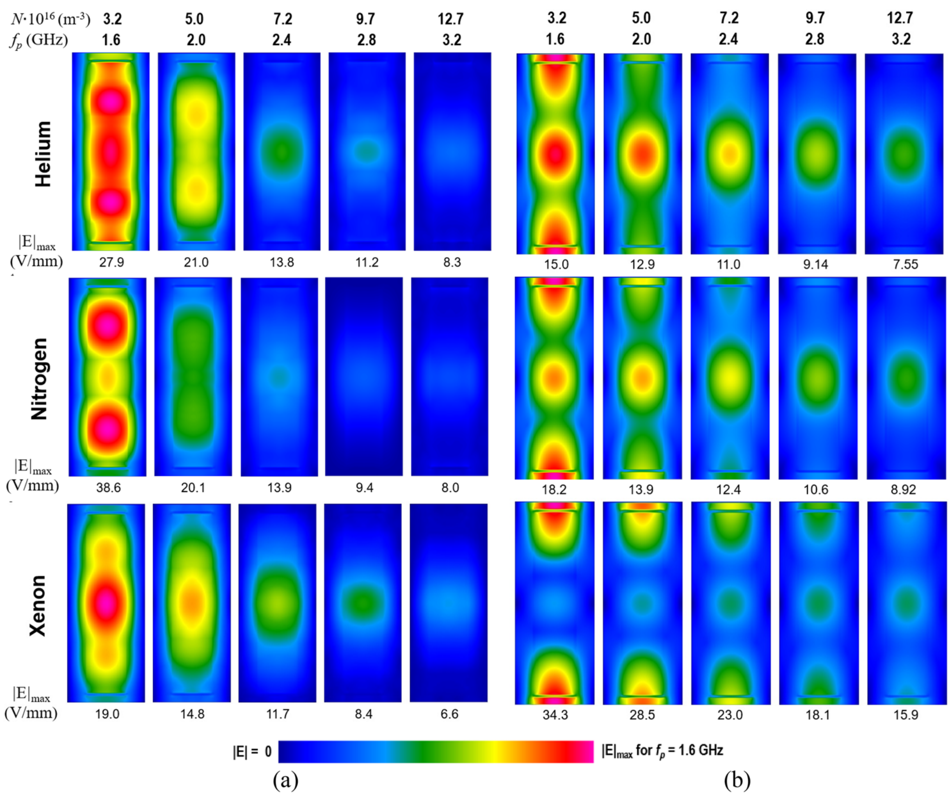

Figure 6. Patterns of the electric field relative to the maximum value of the field's magnitude $|E|_{max}$ (at $f_p = 1.6$ GHz); the values of $|E|_{max}$ are given next to each pattern. The fields are visualized in the central xz-plane of the system with the cross-sectional excitations [Figure 5(a)] for three gases and different values of plasma frequency f_p; low pressure plasma ($n_g = 1.94 \cdot 10^{22}$ m^{-3}) (a) and atmospheric plasma ($n_g = 2.25 \cdot 10^{24}$ m^{-3}) (b); $f_0 = 2.45$ GHz; $P_0 = 900$ W.

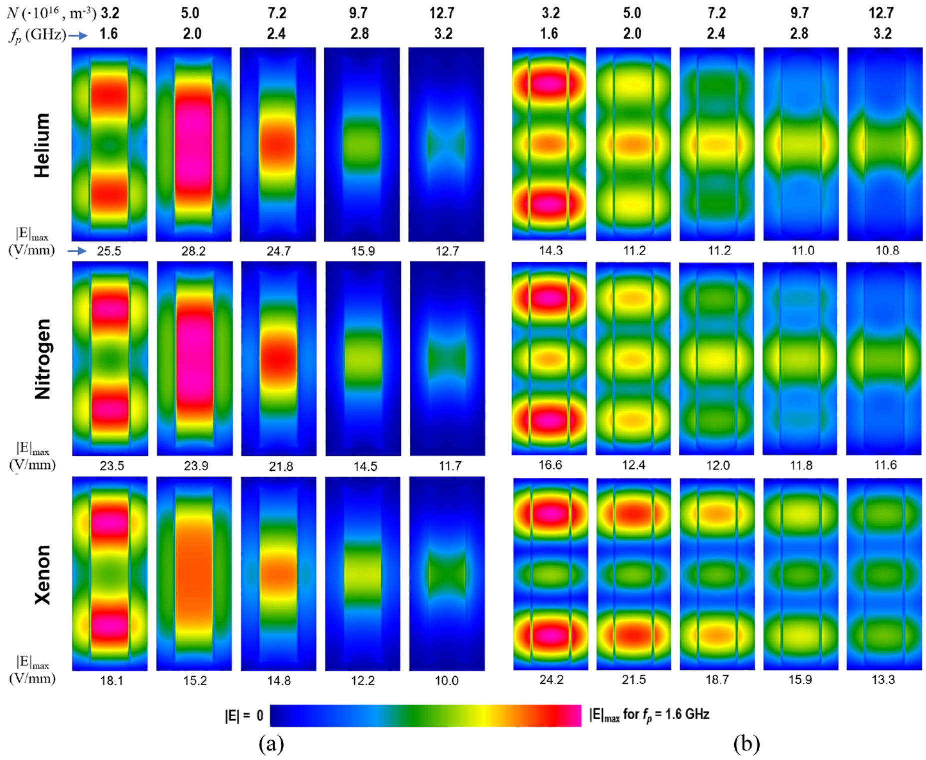

Figure 7. Patterns of the electric field relative to the maximum value of the field's magnitude $|E|_{max}$ (at f_p = 1.6 and); the values of $|E|_{max}$ are given next to each pattern. The fields are visualized in the central xz-plane of the system with the longitudinal excitations [Figure 5(b)] for three gases and different values of plasma frequency f_p; low pressure plasma (n_g = 1.94·10^{22} m^{-3}) (a) and atmospheric plasma (n_g = 2.25·10^{24} m^{-3}) (b); f_0 = 2.45 GHz; P_0 = 900 W.

The patterns in Figures 6 and 7 are consistent with the anticipated behavior of the field with respect to critical plasma frequency. Namely, when $f_p < f_{pc}$, the fields visibly occupy almost the entire interior of the quartz vessel. When $f_p > f_{pc}$, the fields in the central part of the vessel are significantly smaller in magnitude. Depending on the waveguide orientation, gas, and pressure, as f_p increases from 1.6 to 3.2 GHz, $|E|_{max}$ decreases by roughly 1.2 to 5 times. Transformation of the electric field with variation of f_p is shown in more detail in the Appendix. The patterns are presented there for a total of five gases, and a wider range of plasma frequency (0.8 – 4.0 GHz) without cross-normalization.

The decay of the electric field is observed in the applicators with both longitudinal and cross-sectional orientations of the exciting waveguide; however, the profiles of the fields are not alike because the orientation of rectangular waveguides excite different sets of modes in cylindrical cavities. The structure of the field also differs for simulations of low and near-atmospheric pressure, and for simulations of different gases.

The depicted patterns are consistent with those for the electric field in a cylindrical applicator with a coaxial plasma vessel obtained by FEM simulation in Pauly et al. (2022). Both computational illustrations demonstrate the effect of electron density (via the plasma frequency) on electric field penetration. The difference is that in Pauly et al. (2022) the patterns are computed for N of three orders of magnitude about N_c ($10^{15} \leq N \leq 10^{18}$ m^{-3}). In this simulation, electron density is in the range of $3.2 \cdot 10^{16}$ to $1.3 \cdot 10^{17}$ m^{-3} (and $0.8 \cdot 10^{16}$ to $2.0 \cdot 10^{17}$ m^{-3} in the Appendix). As such, our patterns detail the distinctions in the field near the critical value N_c with higher resolution.

3.4. S-parameters

The FDTD model of the applicator in Figure 5 was also used to compute frequency characteristics of the reflection coefficient magnitude $|S_{11}|$ at the input of the exciting rectangular waveguide. In the realm of EM modeling scenarios focused on MW power, such characteristics are used to estimate energy efficiency of the system and assess the options for tuning the system at a nearby resonance (Mechenova and Yakovlev 2004; Murphy and Yakovlev 2010; Celuch et al. 2020; Kumi et al. 2020; Porter et al. 2023).

Figures 8 and 9 show the computed $|S_{11}|(f)$ curves in the applicator for both waveguide orientations, simulated for three gases, and near atmospheric pressure; f_p is considered in the interval of 0.8 to 8.0 GHz (consistent with the results in the

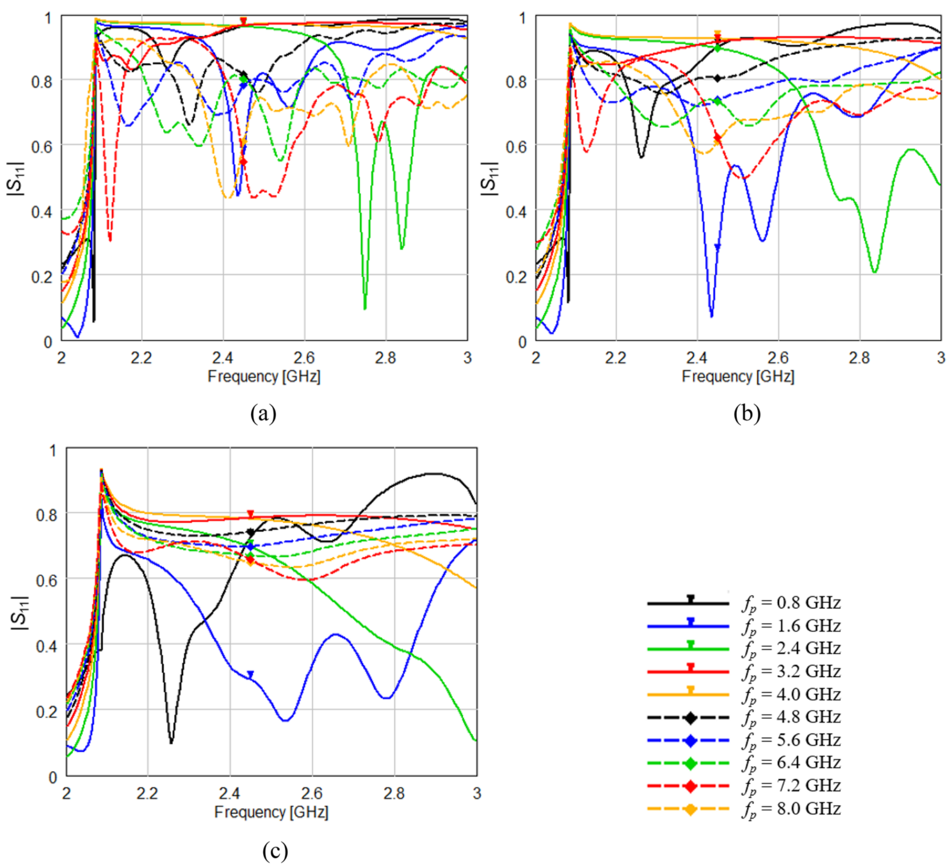

Figure 8. Frequency characteristics of the reflection coefficient $|S_{11}|$ in the system with a cross-sectional excitation [Figure 5(a)] and atmospheric plasma ($n_g = 2.25 \cdot 10^{24}$ m^{-3}) ignited in He (a), N (b), and Xe (c) for different plasma frequencies.

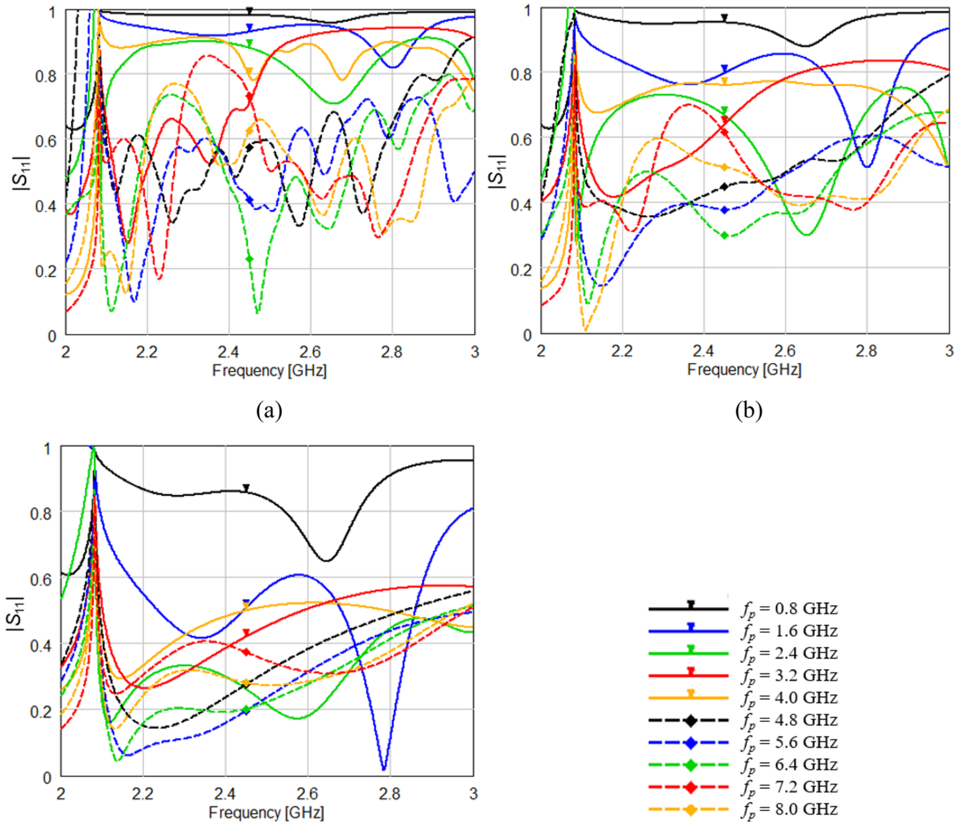

(a) (b) (c)

Figure 9. Frequency characteristics of the reflection coefficient $|S_{11}|$ in the system with a longitudinal excitation [Figure 5(b)] and atmospheric plasma (n_g = 2.25·10^{24} m^{-3}) ignited in He (a), N (b), and Xe (c) for different plasma frequencies.

Appendix); corresponding values of N are within 8·10^{15} to 8·10^{17} m^{-3}. Each curve has a marker highlighting the value of $|S_{11}|$ at f_0 = 2.45 GHz. Overall, lower levels of reflection (and higher coupling with MW plasma) are seen for longitudinal excitation. Unlike the electric field distributions, the characteristics of $|S_{11}|$ are notably different for different gases. It also appears that, in some scenarios, variation of plasma frequency does not make much impact on the $|S_{11}|$ curves [e.g. Figure 8(c)], whereas in others [e.g. Figure 9(a) and (b)] the change is significant. The diversity of curves in Figures 8 and 9 demonstrates instructive potential to tune system parameters for beneficial (or optimal) design of MW systems with plasma in development or prototyping stages.

4. Discussion and conclusion

This paper establishes the legitimacy of FDTD as a time-resolved and computationally efficient alternative for EM modeling of MW plasma. Using a simple model of a cylindrical cavity containing plasma in a coaxial quartz vessel, the approach was demonstrated to simulate the electric field distribution and frequency characteristics of the reflection coefficient for two different waveguide orientations, a broad set of neutral gases, both low- and high-pressure gas densities, and a range of plasma frequency in high resolution about the critical value.

Through the outline of a simple practical approach to characterize MW plasma, this paper collects and presents the necessary information to bridge the critical uncertainty of calculating input parameters from measurable or accessible information about the system. The approach utilizes the conductivity σ, the frequency of electron-neutral collisions γ, and the plasma frequency f_p to perform FDTD EM simulation of the device. These parameters are compatible with FDTD software, which is a necessary condition but not completely sufficient to bridge the uncertainty. Namely, while the dependence of γ and f_p on certain plasma parameters (such as electron density N, neutral gas density n_g, the average electron velocity v_e, and cross-section of collision σ_{en}) can be explicitly calculated, secondary dependance on the device parameters (e.g. MW power, pressure, and gas flow rate) is system specific and usually not known. Here we discussed and demonstrated the steps to generate informative input values by estimation (or measurement) of N, n_g, v_e, and σ_{en}. The presented output includes illustrative simulations of the electric field and the S_{11} parameter which could be used in the early development/design of MW systems with plasma.

Computational results for an example cylindrical MW cavity containing a coaxial cylindrical vessel with plasma (Figure 5) reproduce familiar behavior of the EM field in the presence of plasma and suggest legitimacy of the proposed characterization for plasma medium. When plasma frequency is less than its critical value, $f_p < f_{pc}$ ($N < N_c$), the electric field is present everywhere within the cavity. Otherwise $f_p > f_{pc}$, ($N > N_c$), the field is concentrated outside the plasma domain. The simulated patterns in Figures 6 and 7 and A1-A4 show how, with the increase of electron density in the vicinity of f_{pc}, the field excited by the dominant mode of the rectangular waveguide feeder is transformed and gradually extruded from the plasma. In applications, N is normally higher than in the present computations, however, the values of f_p were chosen to be relatively close to f_0.

This modeling output demonstrates that even using approximated input parameters for plasma, this route of simulation aids in the understanding of system behavior and identify influential parameters for the device's performance. For instance, frequency responses of the reflection coefficient, as evidenced in Figures 8 and 9, suggest that certain geometric and plasma parameters (n_g conditioned primarily by power and f_p conditioned primarily by pressure) may be responsible for tuning the system at a resonance, allowing for high energy coupling. The field patterns demonstrate that the electric field inside and outside plasma volume may depend more on pressure and the system design (system geometry), rather than the gas in which the plasma is ignited and maintained. With the help of such an FDTD EM model, it is possible to obtain concrete means to achieve beneficial functionality of the device, identify trade-off issues, and narrow down a range of possible design options, thus allowing greater preparation for experimental development of the physical prototype. This capability may be further improved using machine-learning algorithms for generalization or optimization of certain parameters or data. One method of this sort is described in Williams et al. (2023) and Williams et al. (2024).

Because of the abovementioned conceptual uncertainty in data on plasma medium, the proposed method to modeling systems with MW plasma must make certain assumptions and simplifications and thus has corresponding limitations. However, the approach is naturally open for further development towards more adequate representation of plasma or more specific plasma cases. Alternative means of calculating the collision frequency, motivated by the focus on certain types of plasma, is one possible suggestion to this end. Another suggestion may be to account for non-uniformity of certain plasma features by attributing a corresponding non-homogeneous FDTD mesh. Cell size can be made as small as physically necessary to adequately represent the scenario if stability of simulation is maintained (*via* consistency of the spatial discretization with corresponding time steps).

In general, it appears that even with principal uncertainties in input data for the plasma medium, the approach (characterization of MW plasma, associated assumptions, and FDTD EM modeling) outlined in this paper is a practical tool to determine the operational bounds of applicators containing plasma and assist in the CAD of such devices.

Acknowledgments

The authors are thankful to Yehia F. Khalil and Srdjan Simunovic for their encouragement and inspirational comments on the topic of this study, John F. Gerling for the valuable commentaries on the design of MW plasma systems, and Raymond L. Boxman for scrupulous reading the draft of the manuscript and useful discussions in the related topics of plasma physics.

Disclosure statement

No potential conflict of interest was reported by the authors.

Notes on contributors

Camille E. Williams is in the fourth year of pursuit of her B.S. degree in Mathematics and Physics from Worcester Polytechnic Institute, Worcester, MA. Her research interests include modeling and applications of microwave plasma, ultrafast photoexcited carrier dynamics, quantum sensing of 2D materials, and antenna technologies in aerospace applications.

Vadim V. Yakovlev has been with the Department of Mathematical Sciences, Worcester Polytechnic Institute, Worcester, MA, holding teaching and research professorships, since 1996. He is the head of the Industrial Microwave Modeling Group, a division of the WPI's Center for Industrial Mathematics and Statistics. He received his PhD degree in Radio Physics from the Institute of Radio Engineering and Electronics of the Russian Academy of Sciences, Moscow, Russia in 1991. His research interests include electromagnetic and multiphysics modeling for microwave power engineering, sustainable technologies involving microwave and millimeter-wave field-matter interaction, microwave plasma and its innovative applications, and machine-learning techniques for optimization and non-destructive testing/imaging.

Funding

The work of C.E.W. was partially supported by the 2022 WPI Summer Training in Arts & Sciences Research (STAR) Fellowship.

ORCID

Vadim V. Yakovlev http://orcid.org/0000-0001-7344-505X

References

Almog IF, Bradley MS, Bulović V. 2011. The Lorentz oscillator and its applications. MIT OpenCourseWare. Cambridge, MA. https://ocw.mit.edu/.

Ashford B, Tu X. 2017. Non-thermal plasma technology for the conversion of CO_2. Current Opinion in Green Sustainable Chem. 3: 45–49. doi:10.1016/j.cogsc.2016.12.001.

Baeva M, Bösel A, Ehlbeck J, Loffhagen D. 2012. Modeling of microwave-induced plasma in argon at atmospheric pressure. Phys Rev E Stat Nonlin Soft Matter Phys. 85 (5 Pt 2): 056404. doi:10.1103/PhysRevE.85.056404.

Bardos L, Barankova H. 2022. Microwave plasma sources and methods in processing technology. Hoboken, NJ.: IEEE Press/Wiley.

Boulos MJ, Fauchais PL, Pfender E, editors. 2023. Handbook of thermal plasmas. New York, NY: Springer Cham. 10.1007/978-3-319-12183-3.

Celuch M, Gwarek WK. 2007. Properties of the FDTD method relevant to the analysis of microwave power problems. J Microw Power Electromagn Energy. 41(4):62–80. doi:10.1080/08327823.2006.11688571.

Celuch M, Kopyt P, Olszewska-Placha M. 2020. Coupled electromagnetic-thermodynamic simulations of microwave heating problems using the FDTD and FEM methods. In: Erle U, Pesheck P, Lorence M, ditors. Development of packaging and products for use in microwave ovens. Amsterdam, Netherlands: Elsevier. p. 459–511.

Chen W, Zhang Y, Wang Y, Zhong Y, Huang K. 2023. A novel high-efficiency microwave plasma multi-ridges field compressed reactor. Phys Plasmas. 30:023502.

Choi SY, Minami W, Kim LH, Kim HJ. 2007. Characteristics of 2.4 GHz microwave plasma by Langmuir probe measurements. SSP. 124-126:1621–1624. doi:10.4028/www.scientific.net/SSP.124-126.1621.

Clementi E, Raimondi DL, Reinhardt WP. 1967. Atomic screening constants from SCF functions. II. Atoms with 37 to 86 electrons. J. Chem Phys. 47(4):1300–1307. doi:10.1063/1.1712084.

COMSOL Multiphysics. 1998–2023. COMSOL AB. www.comsol.com.

Deng L, Zhang G, Liu C, Xie H. 2017. Measurements of gas temperature in microwave plasma at atmospheric pressure by molecular emission spectrometry. IEEE Intern. Conf. on Plasma Science (ICOPS), Atlantic City, NJ, May 2017, doi:10.1109/PLASMA.2017.8496270.

Derkaoui N, Rond C, Gries T, Henrion G, Gicquel A. 2014. Determining electron temperature and electron density in moderate pressure H2/CH4 microwave plasma. J Phys D Appl Phys. 47(20):205201. doi:10.1088/0022-3727/47/20/205201.

Diaz MJ. 2011. Modelling of microwave induced plasmas [Ph.D. Dissertation]. Technische Universiteit Eindhoven.

Grant FA. 1958. Use of complex conductivity in the representation of dielectric phenomena. J. App. Phys. 29(1):76–80. doi:10.1063/1.1722949.

Green KM, Borras MC, Woskov PP, Flores GJ, Hadidi K, Thomas P. 2001. Electronic excitation temperature profiles in an air microwave plasma torch. IEEE Trans Plasma Sci. 29(2):399–406. doi:10.1109/27.922753.

Green KM. 2000. Effects of radius, microwave power, and gas flow rate on the electronic excitation temperature in an atmospheric pressure microwave plasma torch (M.S Thesis). Cambridge, MA: Massachusetts Institute of Technology.

Griffiths DJ. 2020. Introduction to electrodynamics. 24th ed. Cambridge, U.K.: Cambridge University Press

Hagelaar GJM, Hassouni K, Gicquel A. 2004. Interaction between the electromagnetic fields and the plasma in a microwave plasma reactor. J. Applied Physics. 96(4):1819–1828. doi:10.1063/1.1769607.

Heald MA, Wharton CB. 1965. Plasma diagnostics with microwaves. Hoboken, NJ.: John Wiley & Sons Inc.

Huang S, Zhang G, Jie Z, Liu C. 2022. Gas temperature measurements and imaging analysis in atmospheric-pressure microwave air induced plasma torch. IEEE Intern. Conf. on Plasma Science (ICOPS), Singapore, February 2022. doi:10.1109/ICOPS37625.2020.9717948.

Jasinski JM, Zakrzewski Z. 2002. Measurements of neutral gas temperature in microwavetorch plasmas at atmospheric pressure. Czechoslovak J Phys. 52:421–426.

Klute M, Kemaneci E, Porteanu H-E, Stefanović I, Heinrich W, Awakowicz P, Brinkmann RP. 2021. Modelling of a miniature microwave driven nitrogen plasma jet and comparison to measurements. Plasma Sources Sci Technol. 30(6):065014. doi:10.1088/1361-6595/ac04bc.

Kumi P, Martin SA, Yakovlev VV, Hilario MS, Hoff BW, Rittersdorf IM. 2020. Electromagnetic-thermal model of a millimeter-wave heat exchanger based on an AlN: Mo susceptor. COMPEL. 39(2):481–496. doi:10.1108/COMPEL-07-2019-0271.

Latrasse L, Radoiu M, Lo J, Guillot P. 2016. 2.45-GHz microwave plasma sources using solid-state microwave generators. ECR-type plasma source. J Microwave Power Electromag Energy. 50(4):308–321. doi:10.1080/08327823.2016.1260880.

Latrasse L, Radoiu M, Nelis T, Antonin O. 2017. Self-matching plasma sources using 2.45 GHz solid-state generators: microwave design and operating performance. J. Microwave Power Electromag Energy. 51(4):237–258. doi:10.1080/08327823.2017.1388338.

Lebedev YA. 2010. Microwave discharges: generation and diagnostics. J Phys Conf Ser. 257:012016. doi:10.1088/1742-6596/257/1/012016.

Li L, Hu L, Tang P, Chen B, He Z. 2018. A microwave reflection method to determine the complex permittivity of time-varying plasma. 2018 IEEE International Symposium on Antennas and Propagation & USNC/URSI National Radio Science Meeting, Boston, MA, July 2018; pp. 1071-1072. doi: 10.1109/APUSNCURSINRSM.2018.8608620.

Ling S, Moebs W, Sanny J. 2016. Distribution of molecular speeds. In: University Physics 2. Houston, TX: OpenStax.

Masamba WRL, Ali AH, Winefordner JD. 1992. Temperature and electron density measurements in a helium/hydrogen capacitively coupled microwave plasma. Spectrochim Acta, Part B. 47(4):481–491. doi:10.1016/0584-8547(92)80041-E.

Mechenova VA, Yakovlev VV. 2004. Efficiency optimization for systems and components in microwave power engineering. J Microw Power Electromagn Energy. 39(1):15–29. doi:10.1080/08327823.2004.11688505.

Mehdizadeh M. 2015. Microwave/RF applicators and probes: for material heating, sensing, and plasma generation. 2nd ed. Amsterdam, Netherlands: William Andrew.

Möller W. 2006. Fundamentals of plasma physics. Dresden: University of Technology Dresden.

Muegge. 2023. Atmospheric microwave plasma technology – high temperature and power-to-X applications. https://muegge.de/en/atmospheric-microwave-plasma-technology-high-temperature-and-power-to-x-applications/.

Murphy EK, Yakovlev VV. 2010. CAD technique for microwave chemistry reactors with energy efficiency optimized for different reactants. ACES J. 25(12):1108–1117.

Nowakowska H, Jasinski M, Debicki PS, Mizeraczyk J. 2011a. Numerical analysis and optimization of power coupling efficiency in waveguide-based microwave plasma source. IEEE Trans Plasma Sci. 39(10):1935–1942. doi:10.1109/TPS.2011.2163531.

Nowakowska H, Jasinski M, Mizeraczyk J. 2011b. Numerical analysis of tuning procedure of a waveguide-based microwave plasma source. IEEE Trans Plasma Sci. 39(11):2906–2907. doi:10.1109/TPS.2011.2158453.

Ong MY, Nomanbhay S, Kusumo F, Show PL. 2022. Application of microwave plasma technology to convert carbon dioxide (CO_2) into high value products: a review. J. Cleaner Prod. 336:130447. doi:10.1016/j.jclepro.2022.130447.

Pauly S, Schulz A, Walker M, Gorath M, Baumgärtner K, Tovar G. 2022. Modeling and experimental study of remote microwave plasma source for high-rate etching. Chem Ing Tech. 94(3):410–416. doi:10.1002/cite.202100144.

Porter MT, Binner J, Cinibulk MK, Baños BG, Stern KE, Yakovlev VV. 2023. Computational characterization of microwave heating of fibre preforms for CVI of SiCf/SiC composites. J. Eur Ceram Soc. 56(1):1808–1827.

QuickWave. 1998–2024. QWED Sp. z o.o. http://www.qwer.eu.

Shang JJS. 2018. Modeling plasma via electron impact ionization. Aerospace. 5(1):2. doi:10.3390/aerospace5010002.

Shearn M, Sun X, Henry MD, Yariv A, Scherer A. 2010. Advanced plasma processing: etching, deposition, and wafer bonding techniques for semiconductor applications. In: *Semiconductor technologies*. Grym E, editor. Rijeka: InTech; p. 79–104. doi: 10.5772/8564.

Shen Q, Huang R, Xu Z, Hua W. 2020. Numerical 3D modeling: microwave plasma torch at intermediate pressure. Appl. Sci. 10(15):5393. doi:10.3390/app10155393.

Shirai H, Sakuma Y, Ueyama H. 1999. The control of the high-density microwave plasma for large-area electronics. Thin Solid Films. 337(1-2):12–17. doi:10.1016/S0040-6090(98)01167-5.

Shivkumar G, Tholeti SS, Alrefae MA, Fisher TS, Alexeenko AA. 2016. Analysis of hydrogen plasma in a microwave plasma chemical vapor deposition reactor. J. Appl Phys. 119:113301.

Silva F, Hassouni K, Bonnin X, Gicquel A. 2009. Microwave engineering of plasma-assisted CVD reactors for diamond deposition. J Phys Condens Matter. 21(36):364202. doi:10.1088/0953-8984/21/36/364202.

Thomas ELH, Ginés L, Mandal S, Klemencic GM, Williams OA. 2018. A simple, space constrained NIRIM type reactor for chemical vapour deposition of diamond. AIP Adv. 8(3):035325. doi:10.1063/1.5009182.

Toyoda H. 2020. Microwave plasma. In: Horikoshi, S., Serpone, N., editors. RF power semiconductor generator application in heating and energy utilization. Singapore; Springer Nature; p. 181–194.

Ventzek PLG, Rauf S, Stout PJ, Zhang D, Dauksher W, Hall E. 2002. Application and simulation of low temperature plasma processes in semiconductor manufacturing. Appl Surf Sci. 192(1-4):201–215. doi:10.1016/S0169-4332(02)00027-2.

Wang G, Pan H, Lai S, Zhou Y, Wu L, Zhu H, Yang Y. 2021. Dynamic measurement of relative complex permittivity of microwave plasma at atmospheric pressure. Processes, 9, 1812. doi: 10.3390/pr9101812.

Williams CE, Murphy EK, Yakovlev VV. 2024. Machine-learning efficiency optimization of microwave applicators with plasma. EJME. 1(1):44–50. doi:10.18573/ejme.2.

Williams CE, Murphy EK, Yakovlev VV. 2023. Machine-learning efficiency optimization of microwave applicators with plasma. 19th AMPERE Conf. on Microwave and High Frequency Heating, Cardiff, U.K., September 2023; pp. 231–232.

Williams CE, Yakovlev VV. 2023. Characterization of microwave plasma in electromagnetic modeling for processing applications. 57th IMPI's Microwave Power Symp., Denver, CO, June 2023; p. 51–53. Mechanicsville, VA: IMPI.

Wu TJ, Kou CS. 1999. A large-area plasma source excited by a tunable surface wave cavity. Rev Sci Inst. 70(5):2331–2337. doi:10.1063/1.1149759.

Wu X, Zhang W, Wu L, Su Y, Huang K. 2021. A microwave-induced atmospheric-pressure low-temperature linear plasma source based on parallel plate transmission lines. IEEE Trans Plasma Sci. 49(11):3532–3536. doi:10.1109/TPS.2021.3119845.

Xiao W, Huang K, Zhang W, Lin Y. 2016. Modeling of argon plasma excited by microwave at atmospheric pressure in ridged waveguide. IEEE Trans Plasma Sci. 44(7):1075–1082. doi:10.1109/TPS.2016.2568266.

Xiao W, Liao Y, Huang K. 2022a. Measuring electron density of atmospheric microwave plasma jet by microwave perturbation method. IEEE Trans Instrum Meas. 71:1–9. doi:10.1109/TIM.2022.3193173.

Xiao W, Liao Y, Wang F, Zhang Z, Zhu H, Yang Y, Huang K. 2022b. Determining electron density of atmospheric microwave air plasma torch by microwave power measurement. IEEE Trans Plasma Sci. 50(6):1781–1789. doi:10.1109/TPS.2022.3173372.

Yadav HNS, Kumar M, Kumar A, Das M. 2021. COMSOL simulation of microwave plasma polishing on different surfaces. Mater Today Proc. 45(6): 4803–4809. doi:10.1016/j.matpr.2021.01.266.
Yakovlev VV. 2006. Examination of contemporary electromagnetic software capable of modeling problems of microwave heating. In: Willert-Porada M, editors. Advances in microwave and radio frequency processing. Berlin: Springer Verlag; p. 178–190.
Yakovlev VV. 2018. Effect of frequency alteration regimes on the heating patterns in a solid-state-fed microwave cavity. J. Microwave Power & Electromagnetic Energy. 52(1):31–44. doi:10.1080/08327823.2017.1417105.
Yakovlev VV, Allan SM, Fall ML, Shulman HS. 2011. Computational study of thermal runaway in microwave processing of zirconia. In: Tao J., editor. Microwave and RF power applications. Toulouse: Cépaduès Editions; p. 303–306.
Zhang W, Tao J, Huang K, Wu L. 2017. Numerical investigation of the surface wave formation in a microwave plasma torch. IEEE Trans Plasma Sci. 45(11):2929–2939. doi:10.1109/TPS.2017.2759501.
Zhang Q, Zhang G, Wang L, Wang X, Wang S, Chen Y. 2009. Measurement of the electron density in a microwave plasma torch at atmospheric pressure. Appl Phys. Let. 95:201502.
Zhong N, Wei X, Zhong Y, Wang Y, Chen W, Huang K. 2023. A novel self-excited atmospheric pressure microwave plasma jet using rectangular coaxial line. IEEE Trans Plasma Sci. 51(5):1239–1246. doi:10.1109/TPS.2023.3264699.

Appendix

Patterns assembled in this Appendix aim to demonstrate the capabilities of the introduced computational approach for analysis of the electric field in MW systems containing plasma. To this end, Figures A1–A4 can be seen as modified and extended versions of Figures 6 and 7. Distributions of the electric field inside the cylindrical applicator (Figure 5) are shown for five different gases and nine values of plasma frequency. The patterns are visualized as relative distributions rather than being normalized to the maximum field value in the set of patterns. Maximum field values accompany each pattern to show the decrease of field magnitude with increasing plasma frequency.

In applications, electron density is heavily conditioned by MW power; the exact dependency of N on P_0, however, is system-dependent and *a priori* unknown. As all simulations of the electric field in Figures A1–A4 (as well as in Figures 6 and 7) mean to demonstrate the computational approach rather than mimic a particular practical device, we assume for simplicity, that the power level is constant despite variation of the electron density (and hence variation of plasma frequency). This assumption more affects the computed values of $|E|_{max}$ than the relative profiles of the patterns. Additionally, experimental data on $N(P_0)$ in Zhang et al. (2009) and Xiao et al. (2022a) imply that the change of f_p from 0.8 to 4.0 GHz may require an insignificant increase of power regardless. In the case that simulations of the electric field are performed in the scenario in which the dependency N (P_0) is known, the input values of f_p for the plasma medium should simply be set up in accordance with this relation.

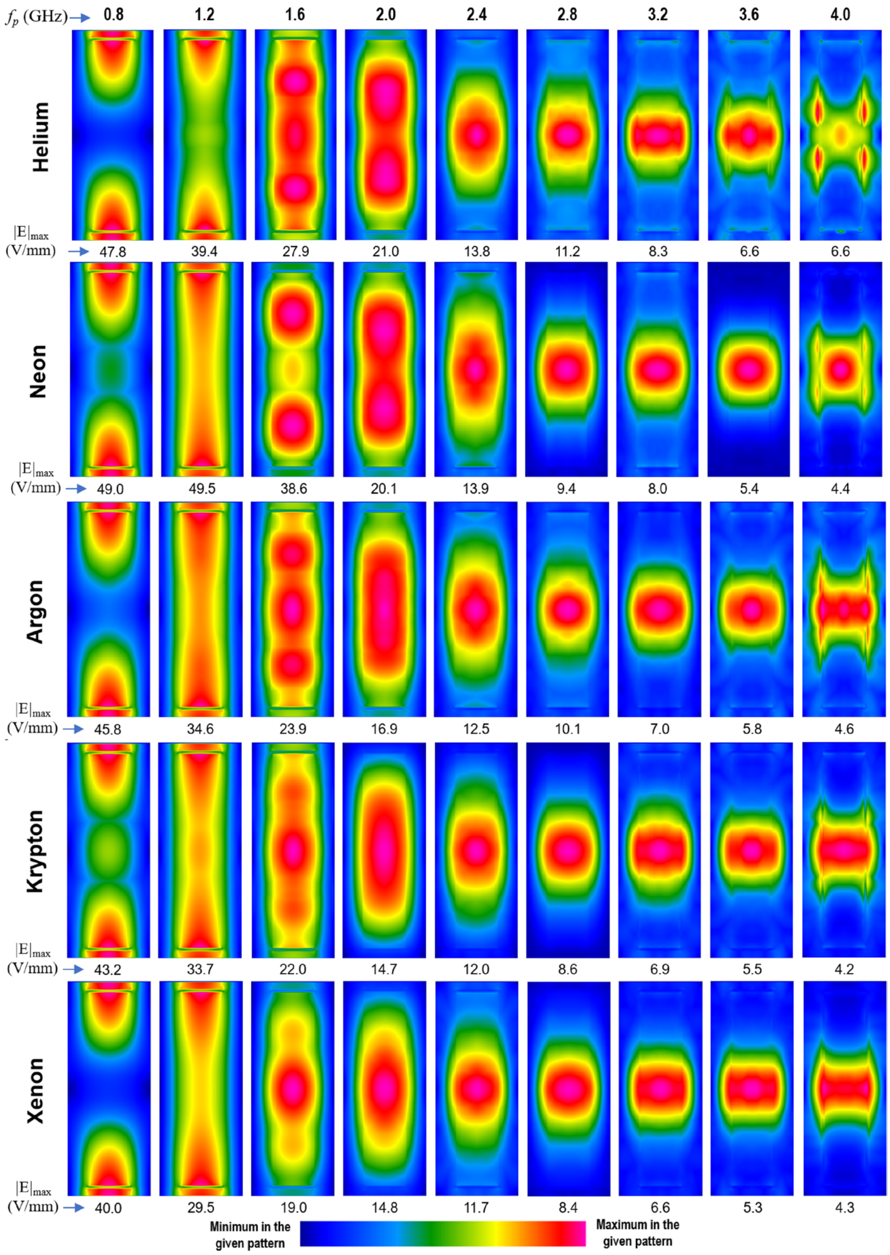

Figure A1. Relative patterns of the electric field |E| in the central *xz*-plane of the system with cross-sectional excitation [Figure 5(a)] for five gases and different values of plasma frequency f_p; each pattern is shown with its maximum values of |E|; low pressure plasma (with $n_g = 1.94{\cdot}10^{22}$ m^{-3}); $f_0 = 2.45$ GHz; $P_0 = 900$ W.

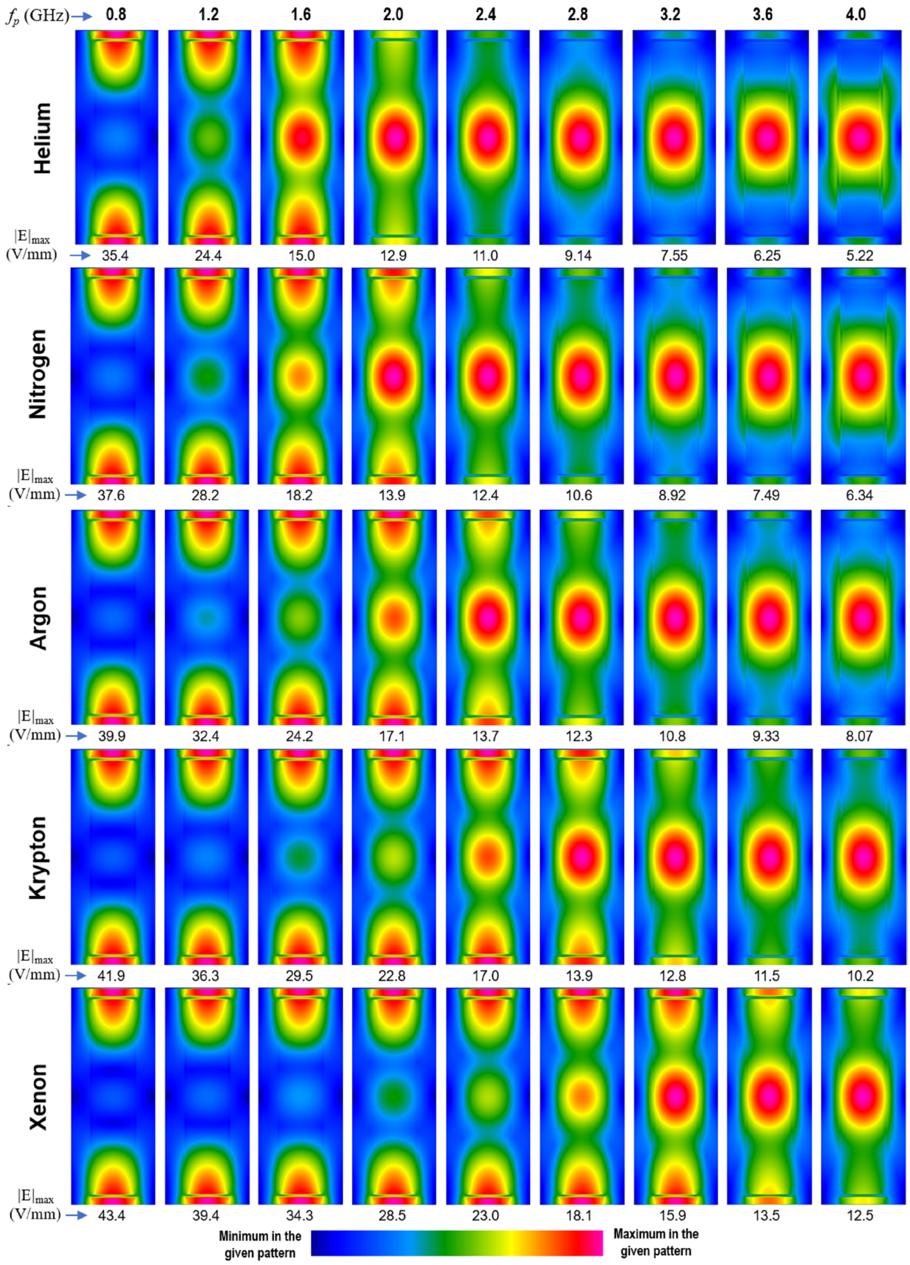

Figure A2. Relative patterns of the electric field |E| in the central *xz*-plane of the system with cross-sectional excitation [Figure 5(a)] for five gases and different values of plasma frequency f_p; each pattern is shown with its maximum values of |E|; atmospheric plasma ($n_g = 2.25 \cdot 10^{24}$ m^{-3}); $f_0 = 2.45$ GHz; $P_0 = 900$ W.

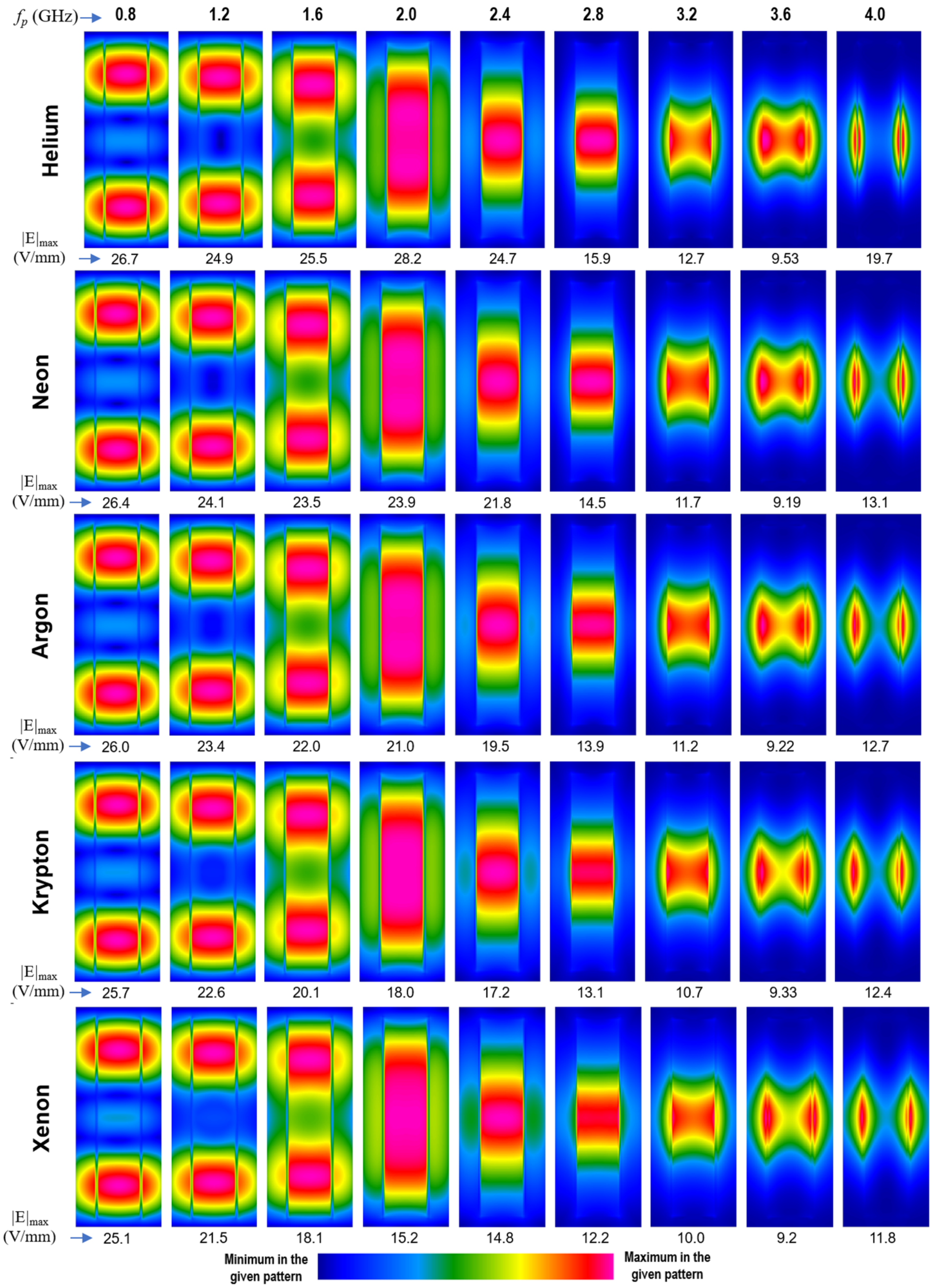

Figure A3. Relative patterns of the electric field |E| in the central *xz*-plane of the system with longitudinal excitation [Figure 5(b)] for five gases and different values of plasma frequency f_p; each pattern is shown with its maximum values of |E|; low pressure plasma (with n_g = 1.94·10^{22} m^{-3}); f_0 = 2.45 GHz; P_0 = 900 W.

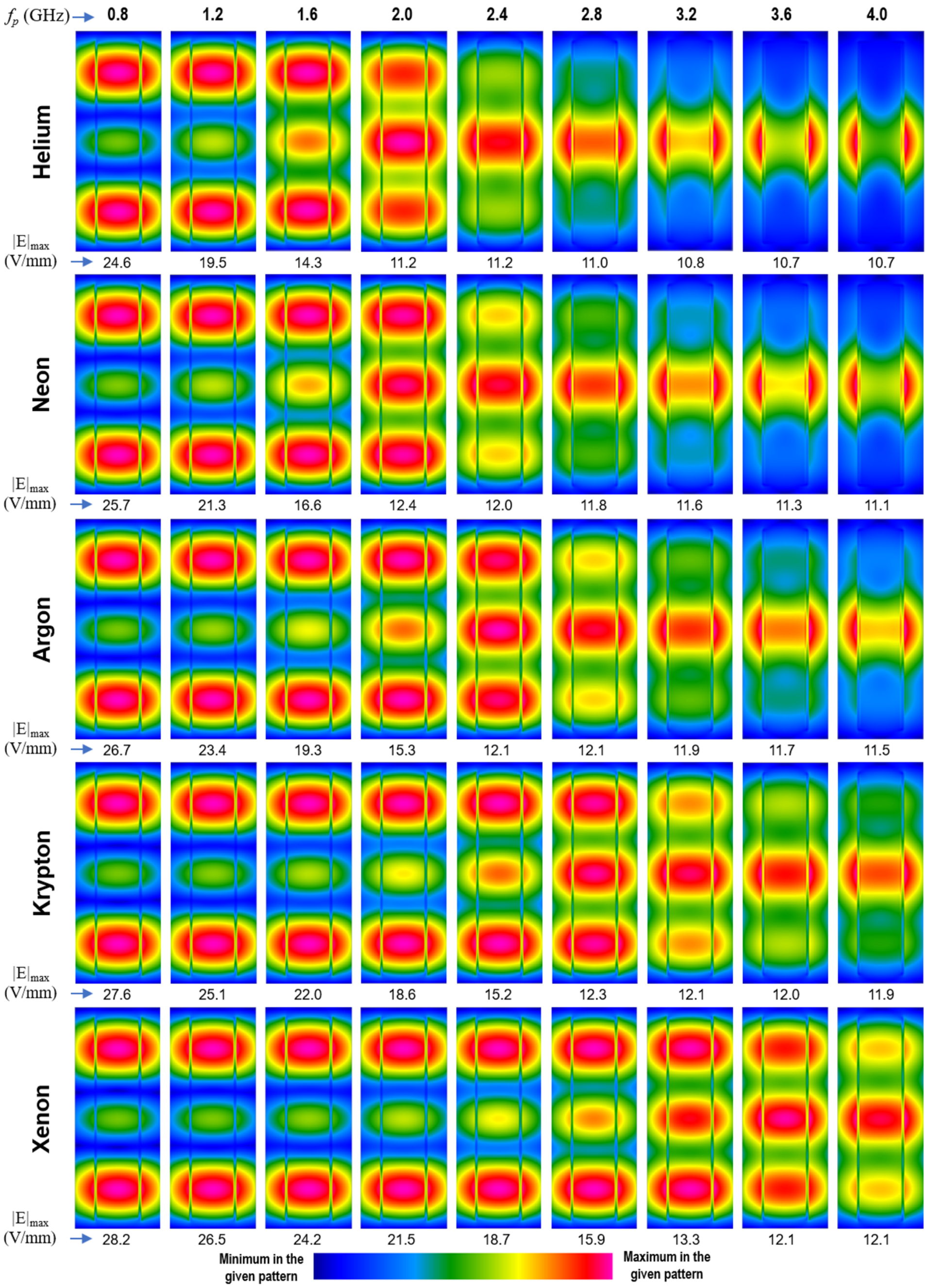

Figure A4. Relative patterns of the electric field |E| in the central *xz*-plane of the system with longitudinal excitation [Figure 5(b)] for five gases and different values of plasma frequency f_p; each pattern is shown with its maximum values of |E|; atmospheric plasma (n_g = 2.25·10^{24} m^{-3}); f_0 = 2.45 GHz; P_0 = 900 W.